Title: Oxygen octahedral tilt ordering in $(Na_{1/2}Bi_{1/2})TiO_3$ ferroelectric thin films

A. Pramanick,[1,*] A. R. Paterson,[2] L. Denis,[3] W. Abbas,[1] G. Niu,[4,*] W. Ren,[4] J. Zhao,[4] L. Dai,[4] O. Borkiewicz,[5] Y. Ren,[5] D. Ho,[1] S. Trolier-McKinstry,[3] and J. L. Jones[2]

[1]*Department of Materials Science and Engineering, City University of Hong Kong, Kowloon, Hong Kong SAR, China*
[2]*Department of Materials Science and Engineering, North Carolina State University, Raleigh, NC 27695, USA*
[3]*Department of Materials Science and Engineering, Pennsylvania State University, University Park, PA 16801, USA*
[4]*Electronic Materials Research Laboratory, Key Laboratory of the Ministry of Education and International Center for Dielectric Research, School of Electronic Science and Engineering, Xi'an Jiaotong University, Xi'an 710049, China*
[5]*Advanced Photon Source, Argonne National Laboratory, Lemont, IL 60439, USA*
Email: apramani@cityu.edu.hk
Email:gangniu@xjtu.edu.cn

Abstract:
The oxygen octahedra tilt (OOT) transition is the most common type of distortion in inorganic ABO_3 compounds with perovskite crystal structure. The importance of OOT transitions is underlined by accompanying changes in the B-O and A-O bonding environments, which consequently affects the electronic states and hence influences electrical, magnetic and superconducting properties of many perovskite compounds. In recent years, controlled manipulation of OOT order in perovskite thin film ferroelectrics has been attempted through heteroepitaxial strain engineering. The current study demonstrates an alternative approach whereby OOT ordering in a 200 nm thick polycrystalline thin film of $(Na_{1/2}Bi_{1/2})TiO_3$ (NBT) Pb-free ferroelectric is induced by applying electric-field along the 111 octahedral tilt axis, which is furthermore enabled by a strong (111) crystallographic texture normal to the film surface. *In situ* X-ray diffraction reveals electric-field-induced OOT ordering proceeds through nucleation and rapid growth of domains with ordered $a^-a^-a^-$ tilting, followed by an increase of tilt angle within the ordered domains.

Keywords: (ferroelectrics, thin films, materials science, X-ray diffraction)

The perovskite crystal structure of inorganic ABO_3 compounds accommodates various distortions, including stretching of cation-anion bonds and distortion/tilting of the BO_6 octahedra.[1,2] Among these, the oxygen octahedra tilt (OOT) transition is the most common type of structural distortion observed in the perovskite family.[3,4] OOT transitions are accompanied by changes in the B-O and A-O bonding environments, which consequently affect the electronic states. For example, OOT can change the B-site point symmetry and hence modify the Jahn-Teller distortions associated with crystal-field splitting of *d* orbitals,[5] or can break inversion symmetry by inducing co-operative A-O displacements.[6] In addition, for A-site cations with a lone pair of electrons such as Pb^{2+} or Bi^{3+}, OOT directly affects the hybridized states between the oxygen *p* orbitals and *s* orbitals of the neighboring A-site ions.[7,8] As a result, OOT order strongly affects the electrical, magnetic and superconducting properties of many perovskite compounds.[5] In recent years, induced OOT ordering has been shown to enable large functional properties, such as magnetoelectric switching in multiferroics[9,10] and enhanced optoelectronic properties of inorganic halide perovskites.[11] Here, electric-field-induced OOT ordering is demonstrated in a 200 nm thick polycrystalline film of piezoelectric $Na_{1/2}Bi_{1/2}TiO_3$ (NBT) with a (111) crystallographic texture.

NBT is a Pb-free ferroelectric material with potential environmental benefits as compared to lead- or niobium-containing ferroelectric oxides.[12,13] The complex structure of NBT with disordered OOT patterns makes it an interesting system to explore field-induced OOT ordering in thin film geometries. The room-temperature crystal structure of NBT was originally described as cubic,[14] whereas more recent diffraction studies suggest a rhombohedral or monoclinic phase.[15,16] Nevertheless, significant differences among its local and average structural states exist,[17,18] which arise from partial occupation of the A-site by Bi^{3+} and Na^+ ions. The small size of these ions causes the oxygen octahedra to tilt. Moreover, unlike Na^+, Bi^{3+} has a lone pair of electrons, which combine with the 2*p* states of the

surrounding O anions,[19] and causes A-site displacements to optimize the bonding environment around the Bi^{3+} ions.[20] The random nature of the local strain fields and local electronic environments can cause unusual combinations of OOT patterns and cation displacements. This may be the origin of the discrepancies in reported tilt systems for NBT. For example, based on neutron powder diffraction analysis, the room temperature tilt system in NBT is reported to be $a^-a^-a^-$ in Glazer notation, which is consistent with an average *R*3*c* phase.[21] The same study also reported a *P*4*bm* → *R*3*c* phase transition upon cooling below 320 °C, causing simultaneous OOT transition from in-phase $a^0a^0c^+$ to an out-of-phase $a^-a^-a^-$.[21] However, since *R*3*c* is not a subgroup of *P*4*bm*, the *P*4*bm* → *R*3*c* phase transition is expected to result in complex microstructural transformations, as reported in transmission electron microscope (TEM) studies of NBT ceramics. Dorcet and Trolliard suggested the existence of retained tetragonal platelets with in-phase $a^0a^0c^+$ octahedral tilting dispersed within the global *R*3*c* phase.[22] Levin and Reaney, however, proposed a continuous tilting model whereby the nanoscale orthorhombic domains with $a^-a^-c^+$ tilting patterns give rise to an average *R*3*c* phase with $a^-a^-a^-$ tilt ordering.[23] The results from recent nuclear magnetic resonance (NMR) spectroscopy studies suggest the presence of a unimodal distribution of octahedral tilting with continuously varying tilt magnitude[24] which is consistent with the model proposed by Levin and Reaney.[23]

Most importantly, the OOT pattern in NBT can be irreversibly altered with the application of electric fields of high amplitude, with consequent effects on dielectric relaxation and enhanced electromechanical properties.[25-31] An electric-field-induced OOT transition is suggested by multiple pieces of data, including changes in superlattice (SL) peak reflections, increases in the relative volume of the ordered *R*3*c* phase, and decreases in diffuse scattering intensity associated with inclusions of the higher temperature *P*4*bm* phase.[32-35] Nevertheless, several questions remain. For example, it is unclear how the tilt pattern evolves

within the majority *R*3*c* phase, particularly at low field amplitudes. Additionally, it is not apparent whether OOT ordering in NBT is of a first or second order nature. Moreover, the possibility of electric-field-induced OOT ordering in thin films of NBT has not been examined until now.

This study demonstrates the electric-field-induced OOT ordering in a 111-textured NBT thin film and examines its transition pathway using *in situ* synchrotron X-ray diffraction. A clear signature for incremental octahedral tilt ordering was obtained from *in situ* monitoring of the ½(311) SL peak reflection during application of an electric field. Concurrent changes in lattice parameters and microstrains were also quantified. Based on the microscopic evidence presented below, it is proposed that the OOT transition in textured NBT film proceeds through nucleation and rapid growth of domains with ordered $a^-a^-a^-$ tilting, followed by an increase of tilt angle and finally a transition to a fully ordered $a^-a^-a^-$ tilt state.

200nm-thick NBT thin films were prepared by the sol-gel method using raw materials of bismuth acetate, sodium acetate, barium acetate and tetrabutyl titanate. 2-methoxyethanol was used as the solvent. Solutions made with 10% excess Na and 2% excess Bi were spin coated onto Pt/Ti/SiO_2/Si substrates. The Pt substrate used exhibited a strong 111 texture (see Supplementary Information). Subsequently, rapid thermal annealing (RTA) at 700 °C for 3 minutes was performed. More details can be found in a previous publication.[35,36] Au top electrodes with a diameter of 500 μm were fabricated using dc sputtering at room temperature.

High-energy X-ray diffraction experiments were done at the Sector 11-ID-C of the Advanced Photon Source (APS) at Argonne National Laboratory. The X-ray wavelength was 0.1173 Å, and the beam size used was 0.1 mm in height and 0.5 mm in width. The thin film sample was mounted on a custom sample stage, with a sample-to-detector distance of 1.8 m. The film was oriented so that the normal to the film surface was perpendicular to the direction

of the incident X-ray beam (Figure 1(a)). After alignment, the sample was tilted by ~1° relative to the incident beam to increase the sample volume irradiated by the beam. *In situ* diffraction experiments were performed under stepwise increments of applied electric fields at both room temperature and at 100 °C. An Oxford Cryostreams 700 instrument precalibrated for temperature accuracy within the experimental settings was used to heat the film. The electric fields were applied through tungsten probe tips contacting the top and bottom electrodes of the sample. A Hewlett Packard 4140B pA meter/dc voltage source was used to apply the voltage through the Signatone DC micropositioners and a Hewlett Packard 4192A LF Impedance Analyzer was used to confirm electrical connection. The voltage was increased in steps of 0.05 V and the collection time at each voltage step was 1 minute. Prior to each measurement, the field was stabilized for ~ 40 s. The applied electric field amplitudes are below the coercive field for domain switching for the thin film sample, which is estimated to be ~ 10 MV/m from macroscopic polarization-electric-field loops.[35]

The diffraction patterns were measured in transmission mode. The wavevectors for the measured scattering patterns were approximately perpendicular to the incident X-ray beam direction. The diffraction image indicated a strong 111-texture normal to the film surface, which is likely facilitated by the 111 texture of the underlying Pt substrate. The one-dimensional peak profiles for *hkl* lattice reflections within the various azimuthal sectors, as marked in Figure 1(b), were obtained from diffraction images using the software Fit2D.[37] Interestingly, the appearance of ½(311) SL reflection upon application of electric fields was observed only at 100 °C, as shown in Figures 1(c,d). For quantitative analysis of the ½(311) SL peak, the 2-D Debye-Scherrer ring was segmented into azimuthal bins of 10° width. The total SL peak intensity was then obtained as a summation of SL peak intensities of all the azimuthal bins, weighted by respective differential solid angle values $d\omega = \sin\varphi d\varphi$, where φ is the angle from the normal to the film surface. After normalization with respect to the

differential solid angles, an angular dependence is noted for the SL peak intensity: the normalized SL peak intensity is absent parallel to the electric field direction, whereas it increases with increase in angle to the electric field direction, as shown in Figure 2(e). The angular dependence of SL peak intensity is however not uniform, the origin of which is not clear at the moment. The total integrated intensity of the ½(311) reflection showed a gradual increase with increase in the applied electric field (Figure 2(a)). The appearance of the ½(311) reflection indicates formation of regions with ordered antiphase $a^-a^-a^-$ octahedral tilts.[20] At the same time, no significant intensity was observed for ½(ooe) reflections, where e is an even integer, which indicates the absence of in-phase $a^0a^0c^+$ tilting at length scales large enough to be observed in a diffraction experiment.

The increase in ½(311) SL peak intensity could be due to an increase in the coherence length of regions with ordered $a^-a^-a^-$ tilts or an increase in the tilt angle of the oxygen octahedra, or a combination of both. To distinguish between these effects, we further analyzed the full-width-at-half-maximum (FWHM) and integrated intensities of the ½(311) SL peak. The SL peak profiles were best fit using a Pearson VII function. The coherence length of regions with ordered $a^-a^-a^-$ tilts is inversely proportional to the width of the ½(311) SL peak. At low fields below 4.5 MV/m, the peak is very broad and the FWHM could not be determined accurately. However, for higher fields, the FWHM is observed to be relatively unchanged as shown in Figure 2(d), which indicates that the coherence length for the OOT order has stabilized. The instrumental broadening is estimated to be on average ~0.074 nm^{-1}, with a small variation of ±0.008 nm^{-1} between the various azimuthal sectors. After taking into account instrumental broadening, the coherence length for OOT order is estimated to be l ~ 50 nm based on the Scherrer formula,

$$l \approx 4\pi / FWHM \qquad (1),$$

which is consistent with values reported earlier for bulk ceramics.[38] As shown in Figure 2(d), beyond 4.5 MV/m the FWHM for ½(311) SL peak does not show any appreciable change. Since the coherence length did not change for fields higher than 4.5 MV/m, the increase in SL peak intensity is hypothesized to be due largely to an increase in the octahedral tilt angles. As shown in the original work of Glazer *et al.*,[39] the intensities of the SL reflections are correlated directly to the octahedral tilt angles. For *hkl* reflections, a relationship between the intensity (*I*) and tilt angles α, β and γ about the pseudocubic axes *a*[100], *b*[010] and *c*[001], respectively, is shown in Eqn. 2:

$$I\left(a^{-},b^{-},c^{-}\right)\propto\left[\left(ki^{l}-li^{k}\right)\alpha\pm\left(-li^{h}+hi^{l}\right)\beta\pm\left(hi^{k}-ki^{h}\right)\gamma\right]^{2} \qquad (2)$$

Where $i=\sqrt{-1}$. For $a^{-}a^{-}a^{-}$ tilting where $\alpha = \beta = \gamma = \omega$ and where ω is the tilt angle, $I\left(a^{-},a^{-},a^{-}\right)\propto\omega^{2}$ for the ½ (311) reflection. As shown in Figure 2(d), the ½(311) SL peak intensity for fields lower than 6 MV/m follows a quadratic dependence on field amplitude, which further reinforces the proposition that a gradual rotation of the oxygen octahedra around the [111] tilt axis occurs, followed by a first-order transition to an ordered $a^{-}a^{-}a^{-}$ for a majority of the film volume at ~ 6 MV/m.

The current results resemble field-dependent SL peak intensity changes reported for $0.94(Na_{1/2}Bi_{1/2})TiO\text{-}0.06BaTiO_3$ (NBT-6BT) bulk ceramics, although with some differences.[40] For the bulk ceramic samples, ½(311) SL peak intensity changes were observed under applied electric fields, in conjunction with non-180° domain switching. Furthermore, the ½(311) SL peak intensity changes were irreversible at RT, while at 100 °C they were reversible.[40] In contrast, for the 111-textured NBT thin films, only irreversible changes in ½(311) SL peak intensities are observed at 100 °C, which occurs in the absence of any non-180° domain switching process. Such differences between the field-induced responses in bulk ceramic and thin film samples could be related to their different microstructures and internal stress states.

A one-to-one correspondence between the ½(311) SL peak intensity and the FWHM of the pseudocubic (111) reflection parallel to the electric-field direction (Sector 0°), can also be observed from Figure 2(b). Note that the (111) lattice peak comes from crystallites (or grains) containing domains with both disordered and ordered octahedral tilting, which is unlike the SL peak that comes exclusively from domains with ordered $a^-a^-a^-$ tilting. Consequently, the FWHM of the (111) peak is not sensitive to the size of the domains with ordered $a^-a^-a^-$ tilting. Instead, the factors affecting the FWHM of the (111) peak are X-ray beam width, crystallite size and microstrain. Assuming the beam width and crystallite size remain constant, the change in FWHM of the (111) peak then corresponds to a gradual increase of microstrains within the film. This can be expected as the corner-linked oxygen octahedra are stretched due to inhomogeneous tilt patterns across the film volume. At ~ 6 MV/m, the FWHM abruptly decreases, indicating a lowering of microstrains across the film volume. The first-order like transition at ~ 6 MV/m, combined with an abrupt change in microstrains, indicate that at this stage the strains homogenize. A possible route for strain relief could be a microtwinning mechanism for OOT ordering,[41] which may also partially explain the domain fragmentation observed for NBT during electrical cycling.[38] This should be examined further with detailed microscopic studies.

Evaluating the different lattice strains concurrent with OOT ordering provides further insights into the electric-field-induced structural transition. Figure 1(b) shows the *hkl* pseudocubic peak positions at different directions relative to the electric field. For directions parallel to the electric field (Sector 0°), Figure 2(c) shows a gradual increase in (111) d-spacing for small field amplitudes followed by a sharp increase at ~ 6 MV/m, which correlates to the changes in SL peak intensity and the (111) peak width. Similarly sharp transitions at ~ 6 MV/m are also observed for d-spacings of (*hkl*) lattice reflections with their plane normals at different angles to the electric field, viz. (111) strains at Sector 70°, (002)

strains at Sector 54°, $(01\bar{1})$ strains at Sector 90° and (011) strains at Sector 35°, as shown in Figure 3. Interestingly, for fields lower than 6 MV/m, lattice strains parallel to the electric field direction (i.e. parallel to the [111] tilt axis) show a different trend than the lattice strains away from the field (or tilt) axis. For example, the (111) lattice strains for Sector 0° continuously increase with increasing electric-field amplitudes. However, the lattice strains measured at 45° or more with respect to electric-field exhibit complex trends with a dip at intermediate field levels (2 to 4 MV/m). This can be explained due to the expected difference in induced lattice strains parallel and skewed with respect to the tilt axis. Presumably, the complex nature of the measured lattice strains is due to piezoelectric strain, electrostrictive strain due to rotation of the polarization vector, rotostrictive strain due to octahedral tilting, and complex grain-to-grain interactions or a combination of these effects. Future studies with higher resolution measurements will be necessary to precisely de-convolute these effects.

The atomic mechanism for OOT transitions in NBT films may share similarities with those in rhombohedral $PbZr_{1-x}Ti_xO_3$ or PZT. For $x < 0.4$, below the tilt transition temperature, T_{tilt}, PZT undergoes a transition to an *R*3*c* phase with rotation about the [111] pseudocubic axis to an ordered $a^-a^-a^-$ tilt system.[42,43] In thin films of PZT, octahedral tilt ordering occurs with application of an electric field.[8] The ordering transition for PZT is triggered by short range interactions between the Pb^{2+} ions with a lone pair of electrons and the O^{2-} anions. As Pb^{2+} ions move closer to one of the octahedral faces, they attract neighboring O^{2-} anions, which creates instability in the system and triggers octahedral rotation.[8] This view is consistent with the proposed strong coupling between local polarization vector and octahedral tilt systems in PZT.[44] Similar to Pb^{2+}, Bi^{3+} has a lone pair of electrons that interact with the O 2*p* states. In NBT, the different displacements of Bi^{3+} ions coexist as a broad distribution of polarization vectors.[18] Applied electric fields re-orient these Bi^{3+} displacements, and consequently trigger octahedral rotations through short range interactions

between Bi^{3+} and O^{2-} ions. Notably, the OOT transition in the NBT thin film is only observed at 100 °C, but not at room temperature. This likely results from anharmonic broadening of the phonon modes associated with the vibration of TiO_6 octahedra at elevated temperatures,[45] which would increase the susceptibility for tilting of TiO_6 octahedra.

In summary, the current study offers an alternative approach (e.g. in contrast to interfacial engineering) to induce OOT in thin film ferroelectrics, namely through specifically oriented electric fields in a crystallographically textured film. This approach can be effective if the polarization vector is strongly coupled to the O positions, the clearest example of which are ferroelectrics with A-site ions having a lone pair of electrons, such as Pb^{2+} and Bi^{3+}. The current results also provide insights into the mechanism for electric-field-induced OOT in NBT thin film. Specifically, a gradual tilting of oxygen octahedra occurs, followed by a first-order like transition to an ordered $a^-a^-a^-$ arrangement. This behavior may be generalizable to other materials with disordered octahedral tilts and warrants further studies.

Supplementary Material

Supplementary Information shows X-ray diffraction pattern of NBT film on $Pt/Ti/SiO_2/Si$ substrate, measured using Cu-Kα radiation.

Acknowledgements

AP and WA gratefully acknowledge funding support from CityU (Projects No. 7200514 and 9610377). GN, WR, JZ and LD acknowledge support from the National Natural Science Foundation of China (51602247), Natural Science Fundamental Research Project of Shaanxi Province of China (No. 2017JQ6003), the Fundamental Research Funds for the Central Universities and the Natural Sciences and Engineering Research Council, and Selected Foundation for Science and Technology Activities of Returned Chinese Scholars. STM and LD gratefully acknowledge support from the U.S. National Science Foundation (DMR-1410907). ARP and JLJ gratefully acknowledge support from the U.S. National Science

Foundation (DMR-1409399). This research used resources of the Advanced Photon Source, a U.S. Department of Energy (DOE) Office of Science User Facility operated for the DOE Office of Science by Argonne National Laboratory under Contract No. DE-AC02-06CH11357.

References:

[1] M. E. Lines and A. M. Glass, Principles and Applications of Ferroelectrics and Related Materials, Oxford University Press 1977

[2] K. M. Rabe, C. H. Ahn and J. Triscone, Ed. Physics of Ferroelectrics, Springer 2007

[3] A. M. Glazer, Acta Cryst. B28, 3384 (1972)

[4] P. M. Woodward, Acta Cryst. B53, 32 (1997)

[5] J. M. Rondinelli, N. A. Spaldin, Adv. Mater. 23, 3363 (2011)

[6] Bas B. Van Aken, T. T. M. Palstra, A. Filippetti and N. A. Spaldin, Nat. Mater. 3, 164 (2004)

[7] R. E. Cohen. Nature 358, 136 (1992)

[8] P. Yang, M. A. Rodriguez, G. R. Burns, M. E. Stavig and R. H. More, J. Appl. Phys. 95, 3626 (2004)

[9] Y. Yang, J. Iniguez, A.-J. Mao and L. Bellaiche, Phys. Rev. Lett. 112, 057202 (2014)

[10] H. J. Zhao, M. N. Grisolia, Y. Yang, J. Iniguez, M. Bibes, X. M. Chen and L. Bellaiche, Phys. Rev. B 92, 235133 (2015)

[11] J. S. Bechtel and A. Van der Ven, Phys. Rev. Mater. 2, 025401 (2018)

[12] J. Rodel, K. G. Webber, R. Dittmer, W. Jo, M. Kimura and D. Damjanovic, J. Eur. Ceram. Soc. 35, 1659 (2015)

[13] T. Ibn-Mohammed, I. M. Reaney, S. C. L. Koh, A. Acquaye, D. C. Sinclair, C. A. Randall, F. H. Abubakar, L. smith, G. Schileo, L. Ozawa-Meida, J. Eur. Ceramic Soc. 38, 4922 (2018)

[14] G. Smolenskii, V. Isupov, A. Agranovskaya, N. Krainik, Sov. Phys. Solid State 2, 2651 (1961)

[15] S. Gorfman, P. A. Thomas, J. Appl. Crystallogr. 43, 1409 (2010)

[16] E. Aksel, J. S. Forrester, J. L. Jones, P. A. Thomas, Appl. Phys. Lett. 99, 222901 (2011)

[17] J. Kreisel, P. Bouvier, B. Dkhil, P. A. Thomas, A. M. Glazer, T. R. Welberry, B. Chaabane, M. Mezouar, Phs. Rev. B 68, 014113 (2003)

[18] D. S. Keeble, E. R. Barney, D. A. Keen, M. G. Tucker, J. Kreisel, P. A. Thomas, Adv. Func. Mater. 23, 185 (2013)

[19] H. Thomann, Ferroelectrics 73, 183 (1987)

[20] G. O. Jones and P. A. Thomas, Acta Crystallogr. B56, 426 (2000)

[21] G. O. Jones and P. A. Thomas, Acta Crystallogr. B58, 168 (2002)

[21] V. Dorcet and G. Trolliard, Acta Mater. 56, 1753 (2008)

[22] I. Levin and I. M. Reaney, Adv. Funct. Mater. 22, 3445 (2012)

[23] P. R. Groszewicz, M. Groting, H. Breitzke, W. Jo, K. Albe, G. Buntkowsky and J. Rodel, Sci. Rep. 6, 31739 (2016)

[24] M. Hinterstein, M. Knapp, M. Holzel, W. Jo, A. Cervellino, H. Ehrenberg, H. Fuess, J. Appl. Cryst. 43, 1314-1321 (2010)

[25] Y. Liu, L. Noren, A. J. Studer, R. L. Withers, Y. Guo, Y. Li, H. Yang, J. Wang, J. Sol. State Chem. 197, 309-315 (2012)

[26] C. Ma, H. Guo, S. P. Beckman and X. Tan, Phys. Rev. Lett. 109, 107602 (2012)

[27] B. N. Rao, R. Datta, S. Selva Chandrashekaran, D. K. Mishra, V. Sathe, A. Senyshyn and R. Ranjan, Phys. Rev. B 88, 224103 (2013)

[28] E. Aksel, J. S. Forrester, B. Kowalski, M. Deluca, D. Damjanovic and J. L. Jones, Phys. Rev. B 85, 24121 (2012)

[29] A. R. Paterson, H. Nagata, X. Tan, J. E. Daniels, M. Hinterstein, R. Ranjan, P. B. Groszewicz, W. Jo, J. L. Jones, MRS. Bulletin 43, 600 (2019)

[30] B. N. Rao, A. N. Fitch and R. Ranjan, Phys. Rev. B 87, 060102 (R) (2013)

[31] T.-M. Usher, I. Levin, J. E. Daniels and J. L. Jones, Sci. Rep. 5, 14678 (2015)

[32] J. E. Daniels, W. Jo, J. Rodel, D. Rytz and W. Donner, Appl. Phys. Lett. 98, 252904 (2011)

[33] P. A. Thomas, S. Trujillo, M. Boudard, S. Gordman and J. Kreisel, Solid State Sciences 12, 311 (2010)

[34] S. Gorfman, D. S. Keeble, A. Bombardi, P. A. Thomas, J. Appl. Cryst. 48, 1543 (2015)

[35] J. Zhao, W. Ren, G. Niu, N. Zhang, G. Dong, L. Wang, M. Liu, P. Shi and Z.-G. Ye, ACS Appl. Mater. Interfaces 9, 28716-28725 (2017)

[36] H. F. Ji, W. Ren, L. Y. Wang, P. Shi, X. F. Chen, X. Q. Wu, X. Yao, S. T. Lau, Q. F. Zhou, K. K. Shung, IEEE T Ultrason Ferr 58, 2042 (2011)

[37] A P Hammersley, S O Svensson, M Hanfland, A N Fitch, and D Häusermann, ``Two-Dimensional Detector Software: From Real Detector to Idealised Image or Two-Theta Scan", High Pressure Research, 14, 235-248, (1996)

[38] H. Guo, X. Liu, J. Rodel and X. Tan, Adv. Func. Mater. 25, 270 (2015)

[39] A. M. Glazer, Acta Cryst. A31, 756 (1975)

[40] H. Simons, J. E. Daniels, J. Glaum, A. J. Studer, J. L. Jones, M. Hoffman, Appl. Phys. Lett. 102, 062902 (2013)

[41] V. Dorcet, G. Trolliard and P. Boullay, Chem. Mater. 20, 5061-5073 (2008)

[42] C. Michel, J.-M. Moreau, G. D. Achenbach, R. Gerson and W. J. James, Solid State Comm. 7, 865 (1969)

[43] D. S. Tinberg, R. L. Johnson-Wilke, D. D. Fong, T. T. Fister, S. K. Streiffer, Y. Han, I. M. Reaney and S. Trolier-McKinstry, J. Appl. Phys. 109, 094104 (2011)

[44] D. I. Woodward, J. Knudsen, I. M. Reaney, Phys. Rev. B 72, 104110 (2005)

[45] E. Aksel, J. S. Forrester, B. Kowalski, M. Deluca, D. Damjanovic, J. L. Jones, Phys. Rev. B 85, 024121 (2012)

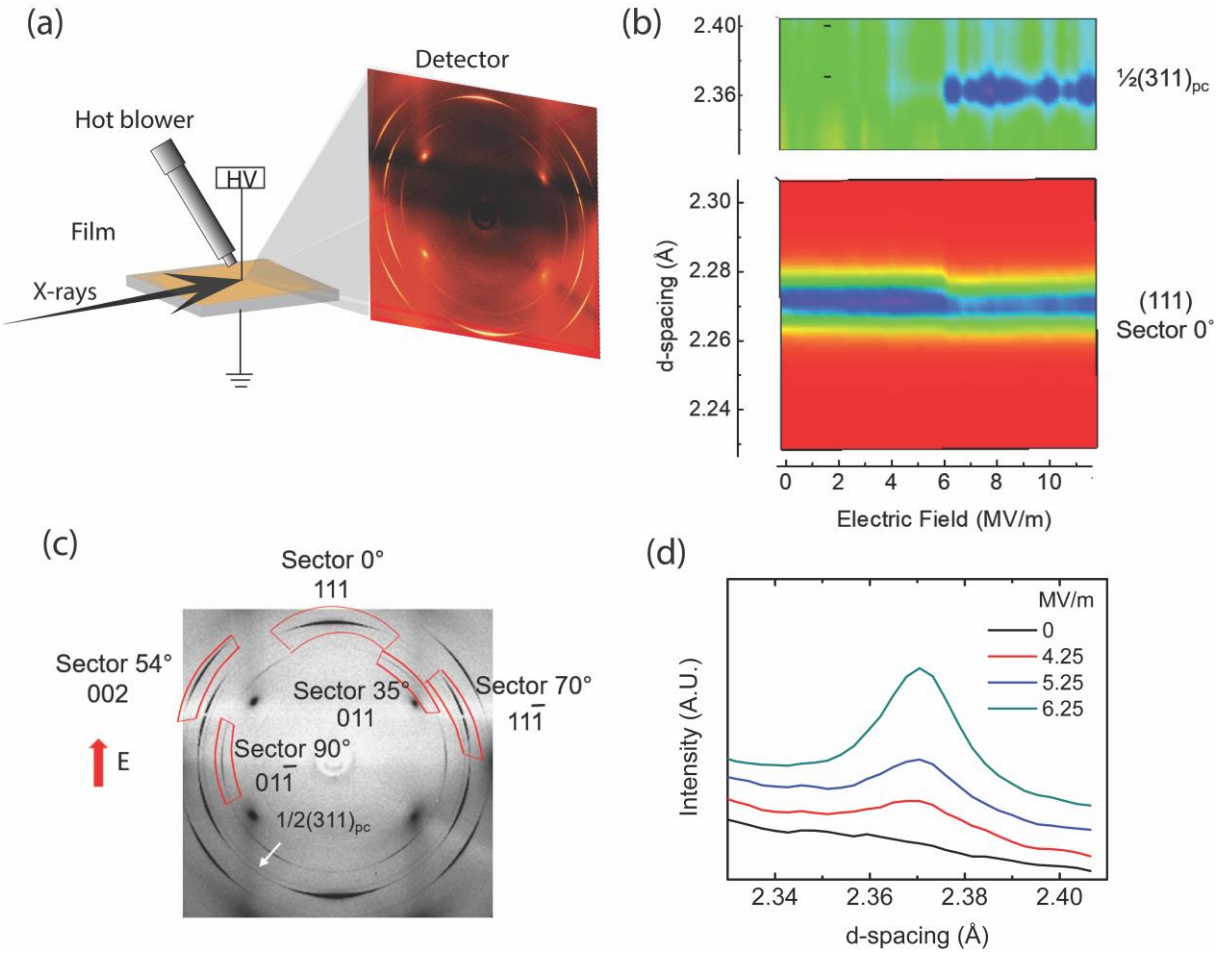

Figure 1: (a) Experimental set up for *in situ* X-ray diffraction under applied electric fields. (b) 2-D diffraction pattern measured at 100 °C. The different sectors are marked based on their nominal angle with respect to the electric field direction. (c) (111) peak and ½(311) SL reflection measured at 100 °C as a function of electric field amplitude. (d) The ½(311) SL peak profile for selected field amplitudes show increase in peak intensity with increasing field amplitude at 100 °C.

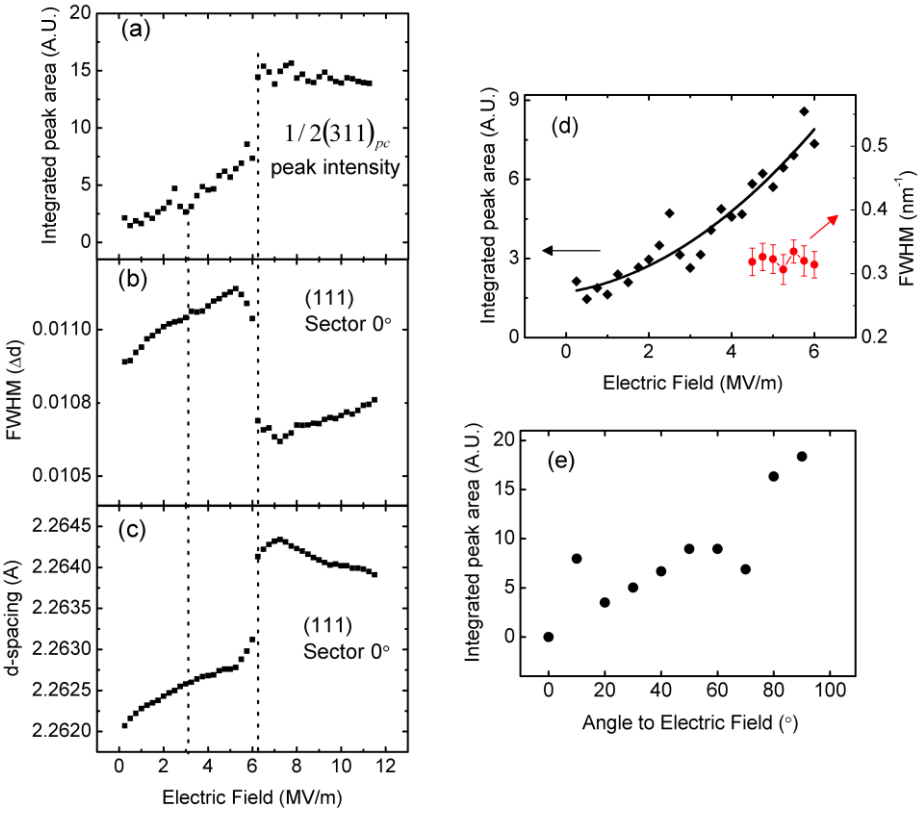

Figure 2: The calculated values for different diffraction peak parameters as function of electric field amplitude: (a) integrated intensity for ½(311) SL peak, (b) peak width of (111) peak and (c) (111) lattice spacing. (d) The integrated ½(311) peak intensity exhibits a quadratic dependence with respect to field amplitude. The FWHM of the SL peak does not show significant change for fields > 4.5 MVm^{-1}. (e) Angular dependence of the ½(311) SL peak intensity with respect to the electric field direction

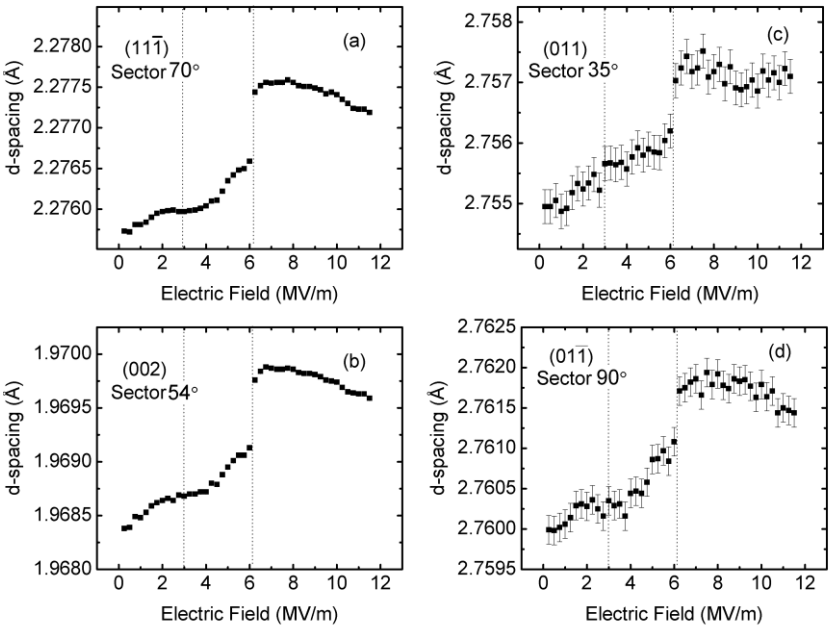

Figure 3: d-spacings measured for different sectors as marked in Fig. 1(b). Electric-field-induced change in d-spacings show different trends for directions parallel (such as shown in Figure 2) and away from the electric field direction.